Optical properties of Mg^{2+}, Yb^{3+}, and Ho^{3+} tri-doped $LiNbO_3$ crystals*

Li Dai(代丽)[1,†], Chun-Rui Liu(刘春蕊)[1], Chao Tan(谭超)[1], Zhe-Hua Yan(阎哲华)[1], and Yu-Heng Xu(徐玉恒)[2]

[1] *Applied Science College, Harbin University of Science and Technology, Harbin* 150080, *China*

[2] *Department of Applied Chemistry, Harbin Institute of Technology, Harbin* 150001, *China*

(Received 10 September 2016; revised manuscript received 20 November 2016; published online 20 February 2017)

A series of $LiNbO_3$ crystals tri-doped with Mg^{2+}, Yb^{3+}, and Ho^{3+} are grown by the conventional Czochraski technique. The concentrations of Mg^{2+}, Yb^{3+}, and Ho^{3+} ions in Mg:Yb:Ho:$LiNbO_3$ crystals are measured by using an inductively coupled plasma atomic emission spectrometry. The x-ray diffraction is proposed to determine the lattice constant and analyze the internal structure of the crystal. The light-induced scattering of Mg:Yb:Ho:$LiNbO_3$ crystal is quantitatively described via the threshold effect of incident exposure energy flux. The exposure energy (E_r) is calculated to discuss the optical damage resistance ability. The exposure energy of Mg(7 mol):Yb:Ho:$LiNbO_3$ crystal is 709.17 J/cm^2, approximately 425 times higher than that of the Mg(1 mol):Yb:Ho:$LiNbO_3$ crystal in magnitude. The blue, red, and very intense green bands of Mg:Yb:Ho:$LiNbO_3$ crystal are observed under the 980-nm laser excitation to evaluate the up-conversion emission properties. The dependence of the emission intensity on pumping power indicates that the up-conversion emission is a two-photon process. The up-conversion emission mechanism is discussed in detail. This study indicates that Mg:Yb:Ho:$LiNbO_3$ crystal can be applied to the fabrication of new multifunctional photoluminescence devices.

Keywords: crystal growth, optical properties, x-ray diffraction, crystal structure

PACS: 42.70.–a, 42.62.Fi, 42.70.Hj, 61.50.Ah **DOI:** 10.1088/1674-1056/26/4/044207

1. Introduction

Lithium niobate ($LiNbO_3$, LN) crystal is widely used as a multifunctional material due to its excellent physical and chemical characteristics such as electro-optic, acoustic-optic, nonlinear optics, piezoelectric, ferroelectric, etc.[1,2] Especially, rare-earth (RE)-doped engineering has attracted considerable attention due to its enormous potential applications in optical communications, optical gyroscopes, optical data storage, laser technology, and remote sensing technology, etc. The rich emission spectrum and unique chemical characteristics of rare-earth ions have been widely studied as the new darling of the laser material.[3–7] Among them, Ho^{3+} which has a special electronic structure has been the most popular activator ion in recent years. Up to now, the up-conversion luminescence properties of Ho^{3+} ions-doped crystals have been extensively investigated. However, the study of the up-conversion luminescence properties of Ho^{3+} ions-doped $LiNbO_3$ crystal is rarely reported.[8,9] In the present paper, Yb^{3+} ion can act as a sensitize ion to increase the up-conversion luminescence intensity of the Ho^{3+} ion because it has a simple energy structure and a long excited state lifetime.[10–12] Nevertheless, a problem for applications of $LiNbO_3$ crystal is that the optical damages will appear when the high-power laser irradiates the pure $LiNbO_3$ crystal or the RE-doped $LiNbO_3$ crystal. Doping anti-photorefractive ions can solve this problem. Many previous studies and experimental results showed that doping Mg^{2+} ions can significantly improve the optical damage resistance ability.[13]

In our experiments, the congruent Yb:Ho:$LiNbO_3$ crystals co-doping different concentrations of Mg^{2+} (1, 3, 5, and 7 mol%) are grown by the Czochralski technique, wherein the concentrations of Ho^{3+} and Yb^{3+} ions are both 1 mol%. The concentrations of Mg^{2+}, Yb^{3+}, and Ho^{3+} ions are measured by an inductively coupled plasma atomic emission spectrometer (ICP-AES). Internal defect structures are studied via x-ray diffraction (XRD). Finally, the light-induced scattering is as a function of exposure energy, and the influences on the defect structures and the optical damage resistance ability of the Mg:Yb:Ho:$LiNbO_3$ crystals with different Mg^{2+} ions doping concentrations are studied. The up-conversion emission spectra, the power pump dependence, and the up-conversion mechanism are measured to understand the influence of Mg^{2+} ion on the up-conversion luminescence of Ho^{3+} ion in Mg:Yb:Ho:$LiNbO_3$ crystal.

2. Experiment

Mg:Yb:Ho:$LiNbO_3$ crystals were successfully grown in air along the *c* direction by the Czochralski technique. The

*Project supported by the National Natural Science Foundation of China (Grant No. 51301055), the Youth Science Fund of Heilongjiang Province, China (Grant No. QC2015061), the Special Funds of Harbin Innovation Talents in Science and Technology Research, China (Grant No. 2015RQQXJ045), and the Science Funds for the Young Innovative Talents of Harbin University of Science and Technology, China (Grant No. 201501).

†Corresponding author. E-mail: daili198108@126.com

© 2017 Chinese Physical Society and IOP Publishing Ltd

doping concentrations of Yb^{3+} and Ho^{3+} ions were 1 mol%, Mg^{2+} ions were 1, 3, 5, and 7 mol% in the melt. The chemicals we used were Li_2CO_3, Nb_2O_5, Yb_2O_3, MgO, and Ho_2O_3 (4N purity) to ensure a high optical quality of the grown crystal. The raw materials were heated up to 750 °C for 2 h to remove the CO_2, and then heated up to 1150 °C for 3 h for a solid reaction. In the growth process, the optimum conditions were chosen as follows: the temperature gradient of the furnace was 30 °C·cm^{-1}–40 °C·cm^{-1}, the pulling rate was 1 mm/h∼2mm/h, and the rotating rate was 20 r/pm∼35 r/pm. Finally, the grown crystals were polarized at 1200 °C with a current density of the 5 mA/cm^2. The polarized crystal was orientational and polished to optical grade. Hereafter, the four samples are denoted as 1#, 2#, 3#, and 4# crystals for convenience.

The concentrations of Mg^{2+}, Yb^{3+}, and Ho^{3+} ions in the Mg:Yb:Ho:$LiNbO_3$ crystals were measured by an inductively coupled plasma atomic emission spectrometer (ICP-AES, Optima 5300DV). The XRD patterns and the lattice constant of Mg:Yb:Ho:$LiNbO_3$ crystal were obtained by an XRD-6000 type x-ray diffractometer (SHIMADZU, Japan) to analyze the structural characteristics.[14,15] Up-conversion emission spectra of Mg:Yb:Ho:$LiNbO_3$ and microsecond time-resolved spectra were measured under excitation at 980-nm semiconductor diode laser.[16] Power dependence was measured by using neutral density filters.

Laser irradiation, even the weak laser pumping source, can cause optical damage as long as the exposure time is long enough. For this situation, Zhang *et al.* proposed a light-induced scattering threshold effect.[17] In the experiment, we adopted a light-induced scattering exposure energy flux threshold method to study the optical damage resistance ability of the samples.[18] The light-induced scattering threshold effect can be quantitatively described by the light intensity value because light-induced scattering is a cumulative effect of the incident light intensity versus time. Therefore, the light-induced scattering threshold effect was proposed to investigate the optical damage resistance ability of the samples. A schematic diagram of the light-induced scattering measurement setup is depicted in Fig. 1. The diode-pumped laser (532 nm) was used as a source, the sample was horizontally polarized, the spot diameter incident on the crystal was 1 mm, and the incident laser power can be adjusted by using an adjustable attenuator. The main role of the diaphragm is to filter scattered light to pass only the central portion of the transmitted light. The diameter of the diaphragm was 1 mm, namely the transmitted beam diameter was equal to the beam diameter incident on the crystal.

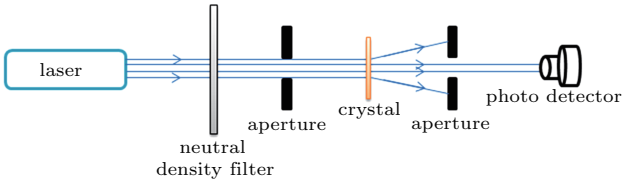


Fig. 1. (color online) Experimental setup for exposure energy flux.

3. Results and discussion

As is well known, the properties of crystalline material are decided by the defect structure. To study the performance, the first thing is to determine the actual concentration of the doping ions in the crystal. The concentrations of Mg^{2+}, Yb^{3+}, and Ho^{3+} ions in the Mg:Yb:Ho:$LiNbO_3$ crystals and the values of effective distribution coefficient (K_{eff}) are listed in Table 1. The values of effective distribution coefficient (K_{eff}) of Mg^{2+}, Yb^{3+}, and Ho^{3+} ions are the concentration percentages in the crystals and melts. The dependence of distribution coefficients of Mg^{2+}, Yb^{3+}, and Ho^{3+} ions on MgO concentration in the melt is shown in Fig. 2.

Table 1. Compositions of Mg:Yb:Ho:$LiNbO_3$ crystals and the optimum growth parameters.

Sample	1#	2#	3#	4#
Mg^{2+} in the crystal/mol%	0.793	2.433	4.215	6.055
K_{eff} of Mg^{2+}	0.793	0.811	0.843	0.865
Yb^{3+} in the crystal/mol%	0.802	0.778	0.743	0.736
K_{eff} of Yb^{3+}	0.802	0.778	0.743	0.736
Ho^{3+} in the crystal/mol %	0.841	0.835	0.820	0.809
K_{eff} of Ho^{3+}	0.841	0.835	0.820	0.809
Crystal size/mm^2	$\Phi 20 \times 25$	$\Phi 25 \times 28$	$\Phi 26 \times 20$	$\Phi 20 \times 20$
Axial temperature gradient/(°C/cm)	30–40	30–35	30–35	25–30
Radial temperature gradient/(°C/cm)	4.5–6.0	4.5–5.0	3.5–4.5	3.0–4.0

It can be clearly seen that the effective distribution coefficient of Mg^{2+} ions increases with increasing MgO concentration in the melt. In addition, the values of effective distribution coefficient of Yb^{3+} and Ho^{3+} ions decrease as the doping concentration of Mg^{2+} increases in their coresponding melts. When Mg^{2+} ion enters into $LiNbO_3$ crystal, it could readily occupy intrinsic defect Nb_{Li}^{4+} site and the Nb_{Li}^{4+} concentration could be reduced. At this time, Ho^{3+} and Yb^{3+} ions have always occupied Nb-bits. When the doping concentration of Mg^{2+} ions reaches or exceeds the threshold concentration, anti-site Nb_{Li}^{4+} is completely substituted. Mg^{2+} ions begin to substitute Li-site and Nb-site of the normal lattice, to

form $Mg_{Nb}^{3-} - 3Mg_{Li}^{+}$ charge balance so that the effective distribution coefficient of Mg^{2+} increases continuously. Nevertheless, the effective distribution coefficients of Yb^{3+} and Ho^{3+} ions decrease sharply, which is ascribed to Mg^{2+}, Yb^{3+}, and Ho^{3+} ions replacing Nb-bits to form Mg_{Nb}^{3-}, Ho_{Nb}^{2-}, and Yb_{Nb}^{2-} which are negative charge excluding each other.

The x-ray diffraction technique is an important means to study the structure of matter. In addition, it can also accurately determine the lattice parameter to perform phase analysis, then study the crystal integrity. Therefore, the lattice constants and lattice structure are the important parameters of x-ray diffraction analysis. The x-ray diffraction patterns of Mg:Yb:Ho:$LiNbO_3$ crystals and experimental results are shown in Fig. 3.

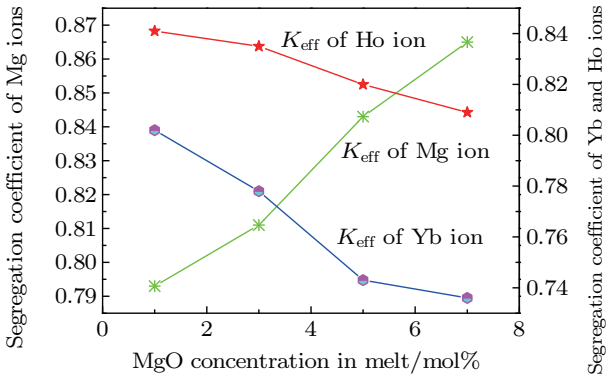


Fig. 2. (color online) Plots of segregation coefficients of Mg^{2+}, Yb^{3+}, and Ho^{3+} ions versus MgO concentration in the melt.

It can be seen from Fig. 3 that the positions of the diffraction peak of four samples are basically similar, and no new diffraction peaks appear. It indicates that the doping Mg^{2+}, Yb^{3+}, and Ho^{3+} ions cause none of their corresponding crystals to significantly change its internal structure, and they are still trigonal systems, like pure lithium niobate crystal. There is no new phase produced, but the radii of doping Mg^{2+} (0.66 Å), Yb^{3+} (0.85 Å), and Ho^{3+} (0.90 Å) ions are different from those of Li^{+} (0.68 Å) and Nb^{5+} (0.69 Å) ions. As is well known, the doping ion radius and defect structure in the crystal will affect the lattice constants and thus the unit cell volume. Therefore, we believe that the doping ions used to substitute Li^{+} and Nb^{5+} ions enter into crystal lattices. According to experimental data, the least squares method is used to calculate the lattice constants of each sample, and the results are shown in Table 2. The lattice constants of congruent $LiNbO_3$ crystal are also listed in Table 2 for comparison, marked as sample 0#. Meanwhile, the unit cell volume V, Δa, Δc, and ΔV are obtained by the formula $V = a^2 c \times \cos 30$. The Δa, Δc, and ΔV can change values of the lattice constant and lattice volume, correspondingly.

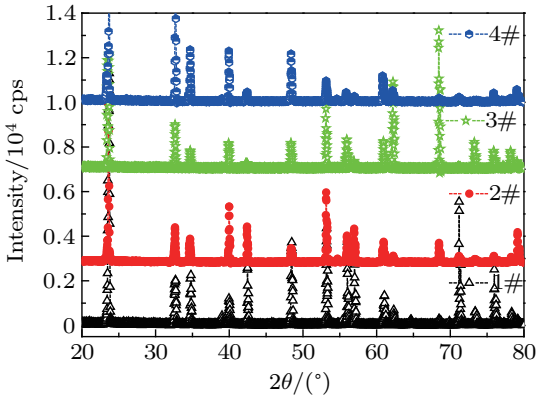


Fig. 3. (color online) The x-ray diffraction patterns of Mg:Yb:Ho:$LiNbO_3$ crystals.

Table 2. Lattice constants of Mg:Yb:Ho: $LiNbO_3$ crystals.

Sample	a/Å	Δa/Å	c/Å	Δc/Å	V/Å^3	ΔV/Å^3
0#	5.1484	0	13.8382	0	317.65	0
1#	5.1513	0.0029	13.8245	–0.0137	317.69	0.04
2#	5.1522	0.0038	13.8509	0.0127	318.41	0.76
3#	5.1551	0.0067	13.8732	0.035	319.28	1.63
4#	5.1519	0.0035	13.8475	0.0093	318.29	0.64

In conjunction with Fig. 3 and Table 2, it is determined that the change of lattice constant is caused by the different Mg^{2+} ions doping concentrations. For samples 1# and 2#, when the Mg^{2+} ions doping concentration is below the threshold concentration, the lattice constants increase slightly; it may be caused by Mg^{2+} ions replacing the anti-site Nb_{Li}^{4+} defects and then occupying Li-sites. In order to make the crystal keep neutral, the reduced is re-occupied by the same number of Li^{+} ions. The oxygen octahedron is expanded because the polarization ability of Nb^{5+} is higher than that of Mg^{2+}so that the volume of the unit cell is expanded. In each of samples 3# and 4#, the doping concentration of Mg^{2+} ions exceeds the threshold concentration (the threshold concentration of Mg^{2+} ions in $LiNbO_3$ crystal is 4.6 mol%), the lattice constants and cell volume both decline. It may be implied that the substitution site of Mg^{2+} changes when the doping concentration of Mg^{2+} ions exceeds the threshold concentration.

In the light-induced scattering test, the intensity irradiated onto the crystal is divided into three parts. Among them, the transmitted intensity received by photo-detector decreases with the increase of exposure time. The relationship between them is shown in Fig. 4. The scattered intensity depending

on the transmitted intensity can be expressed by the following equation

$$I_S = I_{T0} - I_{Tt}, \tag{1}$$

$$R_S = I_S / I_{T0}, \tag{2}$$

where I_{T0} is the transmitted intensity when the laser just starts to irradiate Mg:Yb:Ho:LiNbO$_3$ crystal; I_{Tt} is the transmitted intensity of time t; R_S is the scattering ratio, which is defined as the ratio between scattered intensity and incident intensity, and it represents the intensity of the scattered light.

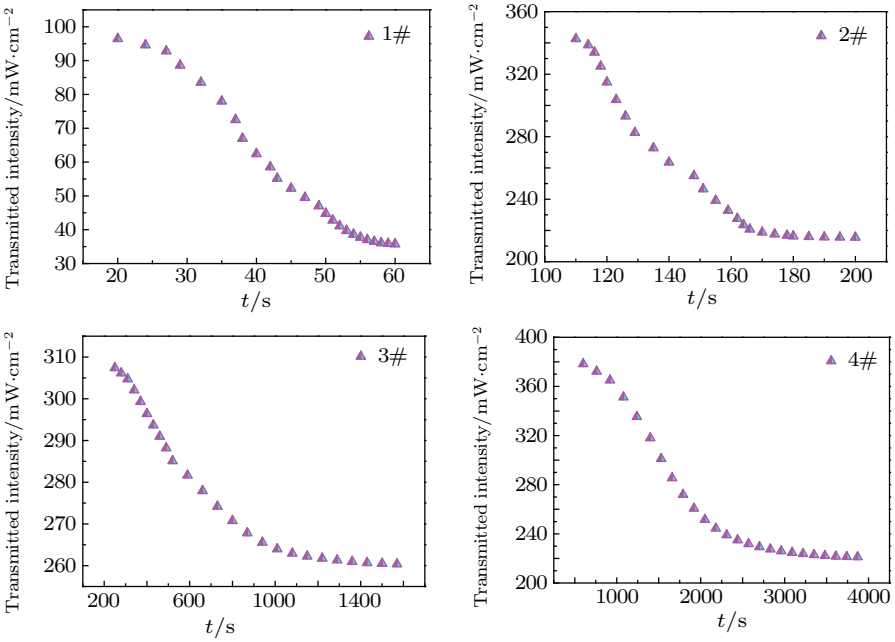


Fig. 4. (color online) Exposure time-dependent transmitted intensities of Mg:Yb:Ho:LiNbO$_3$ crystals.

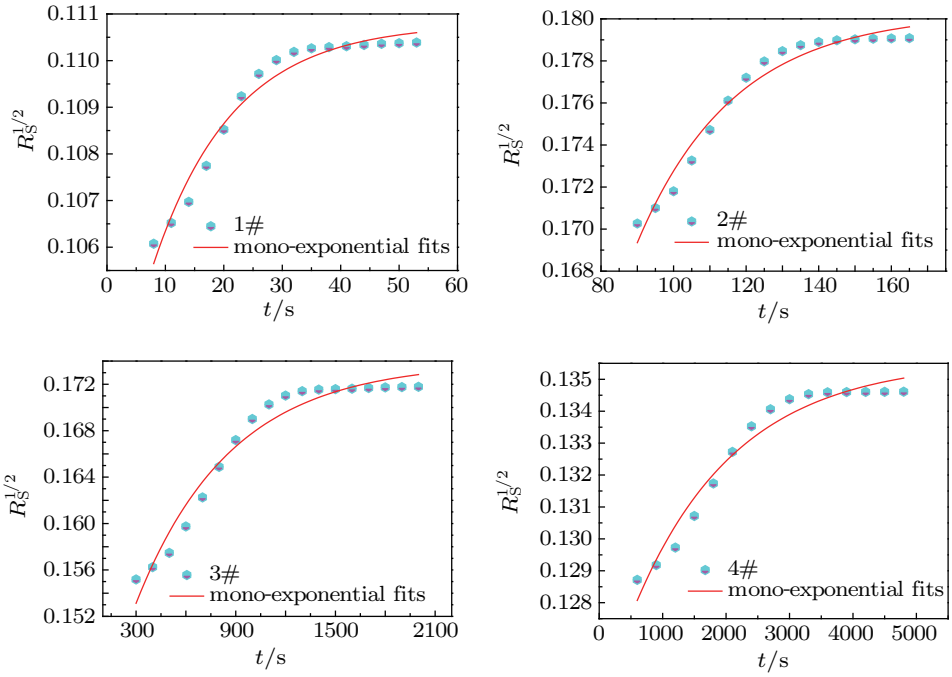


Fig. 5. (color online) Exposure time-dependent square roots of scattering ratio $\sqrt{R_S}$ of Mg:Yb:Ho:LiNbO$_3$ crystals.

The laser light intensity through a lens (I_0) is divided into two parts, one is the effective intensity incident on the crystal (I_{eff}), and the other is the reflection of the crystals (I_R). The relationship between the two is as follows:

$$I_{eff} + I_R = I_0. \tag{3}$$

According to the definition of exposure energy flow, the effective exposure energy flow irradiating the crystal E_r is as follows:

$$E_r = I_{eff}\tau = (1 - R) \times I_0\tau, \tag{4}$$

where R is the reflection index and its value for all samples is

0.1454; τ is the scattering time constant, which represents the required time when the scattering ratio R_s reaches the equilibrium value. The value of τ can be obtained from the curve fitting of the mono-exponential function:

$$\sqrt{R_s}=\sqrt{R_{s.sat}}\left[1-\exp\left(\frac{-t}{\tau}\right)\right], \quad (5)$$

where $\sqrt{R_{s.sat}}$ is the saturation scattering ratio. The relationship between square root of scattering ratio $\sqrt{R_s}$ and exposure time of Mg:Yb:Ho:$LiNbO_3$ crystal is shown in Fig. 5. The experimental data of exposure energy flux for light-induced scattering of Mg:Yb:Ho:$LiNbO_3$ crystals are shown in the following Table 3.

Table 3. Values of light-induced scattering parameters of Mg:Yb:Ho:$LiNbO_3$ crystals, illumination light intensity (I), effective incident intensity (I_{eff}), exposure time (τ), and total exposure energy (E_r).

Crystals	τ/s	I/(mW/cm^2)	I_{eff}/(mW/cm^2)	E_r/(J/cm^2)
1#	13.71	142.66	121.93	1.67
2#	26.73	401.87	343.48	9.18
3#	570.80	445.63	380.88	217.41
4#	1611.38	514.92	440.10	709.17

The effective exposure energy flux (E_r) is used to quantitatively describe the optical damage resistance ability of Mg:Yb:Ho:$LiNbO_3$ crystal. The optical damage resistance ability improves with the value of E_r increasing. As can be seen from Table 3, the exposure energy of sample 4# is biggest, which is about 425 times higher than that of sample 1#. Under the comprehensive comparison, it can be concluded that the Mg^{2+} ions doping concentration of sample 4# is optimal to suppress the light-induced scattering effect.

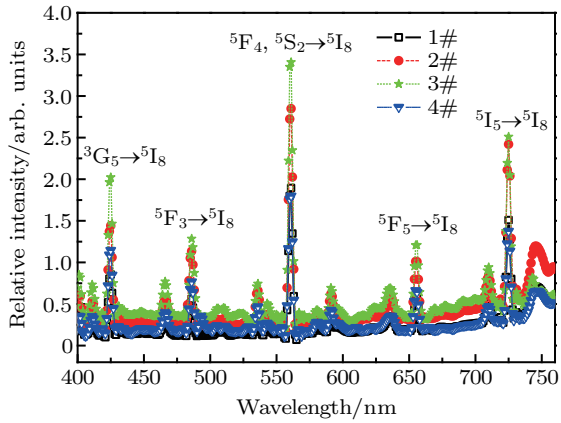


Fig. 6. (color online) Up-conversion emission spectra (400 nm–760 nm, λ = 980 nm) recorded under the same experimental conditions for Mg:Yb:Ho:$LiNbO_3$ samples.

Up-conversion luminescence wavelengths of the Mg:Yb:Ho:$LiNbO_3$ crystals in a range from 400 nm to 760 nm excited with 980-nm LD are shown in Fig. 6. The spectra exhibit five up-conversion luminescence bands centered at approximately 426 nm (violet, medium), 486 nm (blue, medium), 556 nm (kelly, very strong), 654 nm (red, weak) and 727 nm (red, strong), which are attributed to $^5G_5 \rightarrow {}^5I_8$, $^5F_3 \rightarrow {}^5I_8$, ($^5S_2$, $^5F_4$) $\rightarrow {}^5I_8$, $^5F_5 \rightarrow {}^5I_8$, and $^5I_5 \rightarrow {}^5I_8$ transitions of Ho^{3+} ions, respectively.[18]

Figure 7 displays the plots of logarithmic up-conversion intensity versus logarithmic excitation power at 980 nm of Mg:Yb:Ho:$LiNbO_3$ sample. In order to understand the UC mechanism, the pump power dependence of the fluorescent radiation is investigated. The number of photons that are responsible for the upper emitting state can be obtained from the following relation:[20]

$$I_f \propto P^n, \quad (6)$$

where I_f is the fluorescent intensity, P is the pump power, and n is the number of the laser photons required. The n values are obtained from the slope of the plot of $\ln(I_f)$ versus $\ln(P)$. As can be observed from Fig. 7, the value at lower pump power is close to 2, which indicates that a two-photon process is involved in the up-conversion emission.[20]

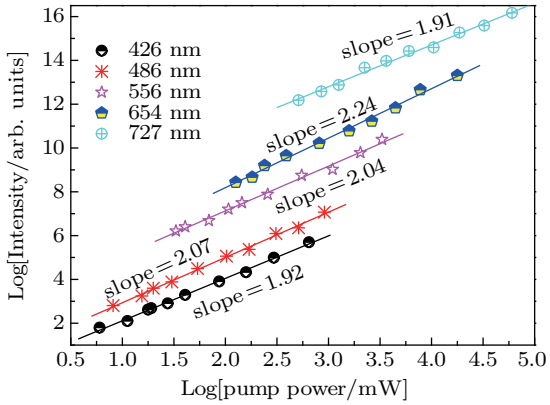


Fig. 7. (color online) Plots of the logarithemic up-conversion intensity versus logarithmic excitation power at 980 nm of Mg:Yb:Ho:$LiNbO_3$ sample.

Schematic energy-level diagrams of Ho^{3+} and Yb^{3+} ions and the up-conversion luminescence mechanism for Mg:Yb:Ho:$LiNbO_3$ crystals are illustrated in Fig. 8. The up-conversion process in Mg:Yb:Ho:$LiNbO_3$ crystal is briefly described as follows. First, the sensitizer Yb^{3+} ions are excited from the $^2F_{7/2}$ to $^2F_{5/2}$ level upon the absorption of NIR photons (980 nm). The ions then transfer energy to the Yb^{3+} ions, excited Yb^{3+} ions populate $^5I_6$, $^5F_4$, $^5S_2$, and $^5G_5$ energy levels of Ho^{3+}. The $^5G_5$ energy levels can drop to $^5F_3$, $^5F_2$, and $^3K_8$ levels via nonradioactive relaxation and via multi phonon relaxation. The $^5F_2$ state relaxes to the $^5F_3$ and $^5S_2$ states in cascade, emitting blue 486 nm ($^5F_3 \rightarrow {}^5I_8$) and green 561 nm ($^5F_4$, $^5S_2 \rightarrow {}^5I_8$) radiations. The partial populations at the $^5G_5$ level directly relax to $^5I_8$ states in cascade, emitting the violet 426 nm ($^5G_5 \rightarrow {}^5I_8$) radiation.

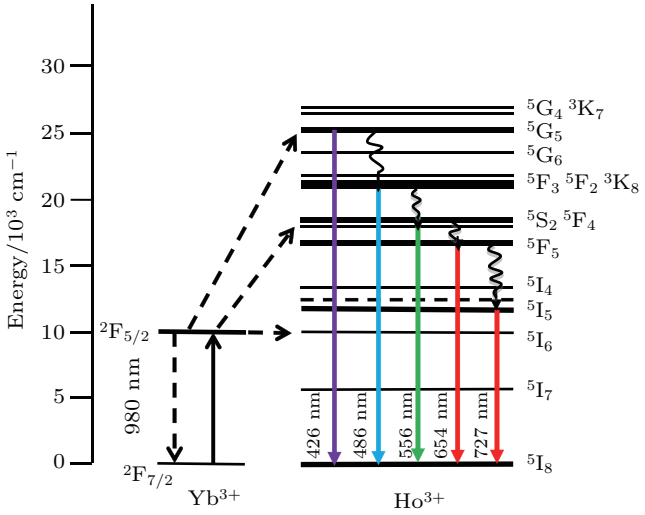


Fig. 8. (color online) Schematic energy-level diagrams of Ho^{3+} and Yb^{3+} ions and the up-conversion luminescence mechanism for Mg:Yb:Ho:$LiNbO_3$ crystals.

Figure 9 shows the dependence of up-converted intensity of the sample on Mg^{2+} concentration under excitation at 980 nm. We can see the up-conversion luminescence intensity of the crystal increases with the increase of Mg^{2+} doping concentration. Our results suggest that the increasing of the doping concentration of Mg^{2+}may be favorable to the electrons located at the $^5G_5$, $^5F_3$, $^5F_4$ ($^5S_2$), $^5F_5$, and $^5I_5$ energy levels, and thereby significantly increases the spectrum transitions from them to the $^5I_8$ level. This is because the incorporation of Mg^{2+} takes the place of the former electron trap, further reduces the rate of non-radiative transition of electrons, improves the luminescence environment of Ho^{3+}, and strengthens the radiation transition.

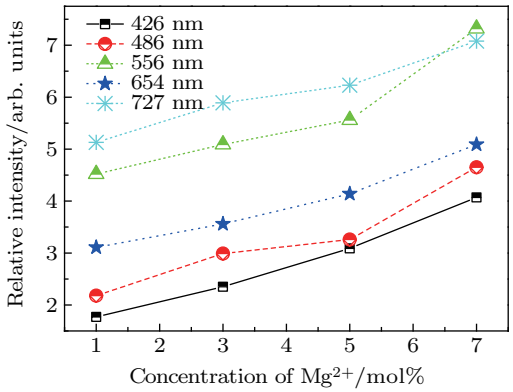


Fig. 9. (color online) Mg^{2+} concentration dependent up-converted intensity of Mg:Yb:Ho:$LiNbO_3$ crystals.

4. Conclusions

In this work, a series of $LiNbO_3$ crystals tri-doped with Mg^{2+}, Yb $^{3+}$, and Ho^{3+} is grown by the Czochralski technique. The effective distribution coefficients of Yb^{3+} and Ho^{3+} ions in the Mg:Yb:Ho:$LiNbO_3$ crystals decrease with the increase of Mg^{2+} ions doping concentration, but Mg^{2+} ions behave oppositely. The XRD results show that no new structural phase is gained, and the lattice constants of samples 1# and 2# slightly increase, and that of sample 3# increases a little more, while that of sample 4# decreases. This suggests that substitution site of Mg^{2+} changes when the doping concentration of Mg^{2+} ions exceeds the threshold concentration. The optical damage resistance ability of Mg:Yb:Ho:$LiNbO_3$ crystal is measured by the light scattering threshold energy flux method. The Mg(7 mol):YbHo:$LiNbO_3$ is the best choice for suppressing the light-induced scattering effect, which has the largest value 709.17 J/cm^2 of E_r, about 400 times higher than that of Mg(1 mol):Yb:Ho:$LiNbO_3$. Five up-converted emission bands are assigned to the transitions $^5G_5 \rightarrow ^5I_8$, $^5F_3 \rightarrow ^5I_8$, ($^5S_2$, $^5F_4$) $\rightarrow ^5I_8$, $^5F_5 \rightarrow ^5I_8$, and $^5I_5 \rightarrow ^5I_8$, respectively. We believe that this paper can promote the understanding of the relations between the Mg^{2+} concentration and the optical properties of Mg:Yb:Ho:$LiNbO_3$ crystal.

References

[1] Weis R S and Gaylord T K 1985 *Appl. Phys. A* **37** 191
[2] WanY B, Yang P Z, WuY R, Zhu H B, Jia T and Hui Y 2007 *Opt. Mater.* **29** 1746
[3] Qian Y N, Xie Z X, Wang R, Zhang H Y and Wu Q B 2015 *Opt. Laser Technol.* **74** 173
[4] Ning K J, Li B Z, Zhang Q L, Hang Y and Shi Z H 2015 *Opt. Commun.* **34** 994
[5] Sreenivasulu A and Buddhudu S 2008 *T. Indian Ceram. Soc.* **67** 129
[6] Chen P, Zhong Z, Jia H, Zhou J, Han J, Liu X and Qiu J 2016 *Rsc Adv.* **6** 7391
[7] Matkovskii A, Potera P, Sugak D, Zhydachevskii Ya, Bolshakova I, Loutts G and Pracka I 2001 *Radiat. Eff. Defects Solids* **155** 61
[8] Sun J Y, Xue B, Sun G C and Cui D P 2013 *J. Rare Earths* **31** 741
[9] Dai L, Li D Y, Xu C, Guo J J and Xu Y H 2013 *Opt. Laser Technol.* **45** 503
[10] Kong J, Tang D Y, Chan C C, Lu J, Ueda K, Yagi H and Yanagitani T 2007 *Opt. Lett.* **32** 247
[11] Dai L, Yan Z H, Jiao S S, Xu C and Xu Y H 2015 *J. Alloys Compd.* **644** 502
[12] Qian Y N, Wang R and Wang B 2012 *Opt. Lett.* **37** 4176
[13] Sun L, Zhao L C and Xu Y H 2008 *J. Chin. Ceram. Soc.* **36** 77
[14] Gao W, Dong J, Wang R B, Wang Z J and Zheng H R 2016 *Acta Phys. Sin.* **65** 084205 (in Chinese)
[15] Liu J, Liu J F, Su L B, Zhang Q, Ma F K, Jiang D P and Xu J 2016 *Acta Phys. Sin.* **65** 054207 (in Chinese)
[16] Zhao H X, Zhao W and Guo Z L 2016 *Acta Phys. Sin.* **65** 064206 (in Chinese)
[17] Zhang G Q, Zhang G Y, Liu S M, Xu J J, Sun Q and Zhang X Z 1998 *J. Appl. Phys.* **89** 4392
[18] Dai L, Tan C, Yan Z H and Xu Y H 2016 *J. Alloys Compd.* **683** 108
[19] Reddy B R, Nash-Stevenson S and Venkateswarlu P 1994 *J. Opt. Soc. Am. B: Opt. Phys.* **11** 923
[20] Pandozzi F, Vetrone F, Boyer J C, Naccache R, Capobianco J A, Speghini A and Bettinelli M 2005 *J. Phys. Chem. B* **109** 17400
[21] Li A H, Zheng Z R, Lu Q, Sun L, Wu W Z, Liu W L, Yang Y Q and Lu T Q 2008 *Opt. Lett.* **33** 1014